Influence of Sample History on the Morphology and Transport Properties of PEO−Lithium Salt Complexes

Maritza Volel* and Michel Armand

International Laboratory on Electroactive Materials, CNRS UMR 2289, Université de Montréal, C.P. 6128, Succursale Centre-Ville, Montréal, Québec H3C 3J7, Canada

Wladimir Gorecki

Laboratoire de Spectrométrie Physique, Université Joseph Fourier, 140 Avenue de la Physique, B.P 87, 38402 Saint Martin d'Hères, France

Received May 14, 2004; Revised Manuscript Received August 8, 2004

ABSTRACT: We provide clear evidence of the effect of the solvent used for sample preparation on the morphology and transport properties of PEO−lithium salt (LiTFSI, $LiBF_4$, or $LiClO_4$) complexes. The surface structure, thermal behavior, and conductivity of the films along with the measured diffusion coefficients and transport numbers of the ionic species are clearly different whether acetonitrile (good solvent of PEO) or methyl formate (poor solvent) was used. Interestingly, the samples with the lowest conductivity have the highest diffusion coefficients, indicative of a difference in carriers concentration. We infer that the polymer chains keep memory of the solvent, and their generated spatial organization is directly implied in conductivity through the use of specific pathways for ionic mobility. Since the variations observed here are of the same amplitude or greater than those observed for some deliberate modification of the polymer electrolytes (i.e., nanoparticles addition, mechanical strain, etc.), great care must now be exercised in giving precise sample history.

Introduction

Polymer electrolytes have long been the center of interest for the development of ideal electrolytes for solid-state lithium batteries.[1−6] They consist of a solvating polymer, usually a polyether, forming a complex with a lithium salt. Conductivity has been associated with the amorphous phases in the system where ionic mobility is dependent on local viscosity and is favored by polymer chain segmental dynamics above the glass transition T_g.[1−6] Strategies to increase conductivity have been based on adjusting the polymer-to-salt ratios and on using salts with a high degree of charge delocalization to generate the widest amorphous domain and lowest T_g.[6] The use of nanoparticle fillers is also extremely popular,[7−9] as they improve conductivity at room temperature along with the mechanical and interfacial properties. It is still controversial whether this is achieved through increased dissociation despite a restriction of chain freedom in the vicinity of the particles. Yet, recent work shows no increase in conductivity for a variety of additives.[10]

Recently, an increase in conductivity has been found also in ordered[11−14] or oriented[15−19] phases, for instance in poly(ethylene oxide) and in other helical or hyperbranched polymers, and is believed to be favored by specific pathways generated by the polymer architecture.

In this study, for the first time to our knowledge, we have explored the effect of the solvent used for film preparation on the morphology (as seen by AFM) and thermal and transport properties (measured by impedance analysis and pulsed-field gradient spin-echo NMR) of the resulting solvent-free films. We considered the case of the well-known poly(ethylene oxide) (PEO) doped with lithium salts of the imide anion, $[(CF_3SO_2)_2N]^-$ (TFSI), ClO_4^-, and BF_4^- cast from two different solvents: acetonitrile (AN) and methyl formate (MF).

* To whom correspondence should be addressed. E-mail: maritza.volel@umontreal.ca.

Experimental Section

Preparation of Samples. Poly(ethylene oxide) ($M_w = 5 \times 10^6$), acetonitrile (99.9% anhydrous), and methyl formate (99.9% anhydrous) were used as received from Aldrich. All salts—LiTFSI (3 M), $LiBF_4$ (Tomiyama), and $LiClO_4$ (Aldrich)—were dried at 150 °C and stored under helium in a glovebox (< −95 °C dew point). These salts were chosen for their favorable phase diagram, ensuring the widest amorphous domains, with the existence of a stoichiometric 6:1 EO unit-to-salt ratio giving low melting eutectics. The respective solvents were added to preweighted amounts of PEO and salt (to give EO unit-to-salt ratios of 20:1) under magnetic stirring in a sealed container. The homogeneous solutions were then centrifuged at 5000 rpm for 15 min (to remove polymerization catalyst residues), and the supernatant was poured into aluminum pans containing pieces of mica or stainless steel plates. After solvent evaporation, the resulting films were dried under vacuum at 60 °C for 24 h and stored in the glovebox for subsequent measurements.

AFM Imaging. A JEOL JSPM-5200 instrument equipped with a vacuum chamber was used. Topography and phase images were acquired on the film-covered mica samples (film approximate thickness: 200 μm) at a clock speed of 666.67 μs, with a resolution of 512 × 512 pixels, under vacuum, in the intermittent contact mode using Olympus silicon probes (length: 160 μm; spring constant: 42 N/m from Asylum Research). The set point voltage was 70% of the free amplitude voltage of the cantilever to allow a medium intermittent contact in order to follow the features without damaging or dragging the sample.

DSC. We used a Pyris 1 Perkin-Elmer differential scanning calorimeter equipped with continuous gas flow in order to prevent sample contamination by humidity. Each sample was weighted in the glovebox, crimp-sealed in an aluminum pan, and kept in the glovebox until right before DSC analysis. For every sample, a first scan was done at 5 °C/min from 20 to 120 °C. The melt was then quenched at 500 °C/min from 120 to −150 °C, and a second scan was then done at 5 °C/min from −150 to 120 °C.

10.1021/ma0490404 CCC: $27.50
Published on Web 09/28/2004

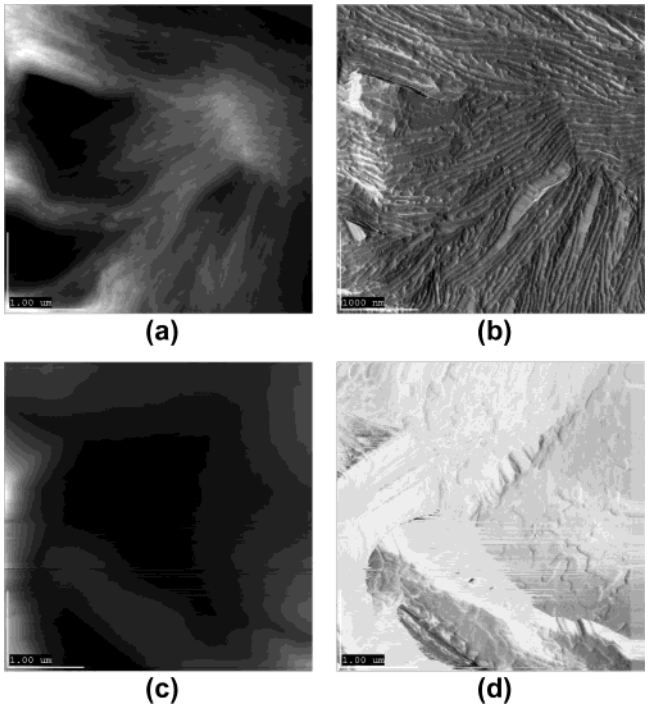

Figure 1. 4 μm × 4 μm AFM images of a PEO film grown from acetonitrile [(a) topography and (b) phase image] and methyl formate [(c) topography and (d) phase image].

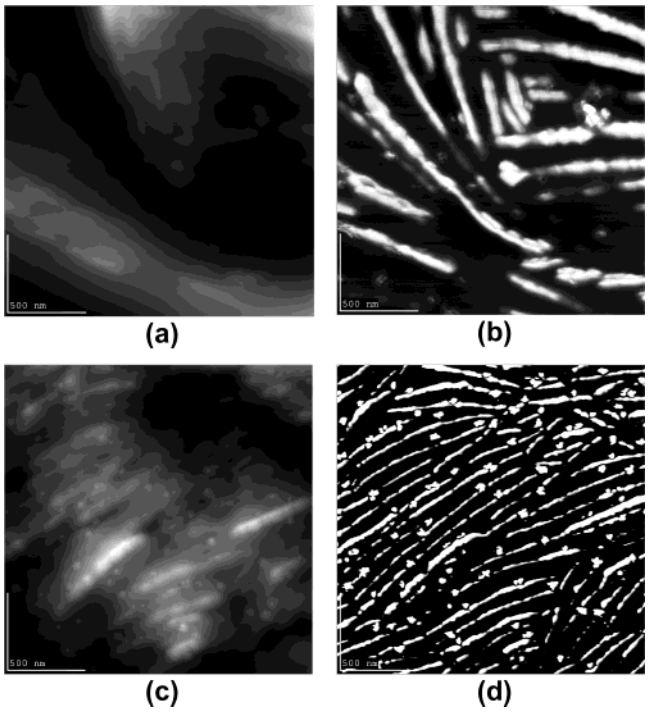

Figure 2. 2 μm × 2 μm AFM images of a PEO:LiTFSI 20:1 film grown from acetonitrile [(a) topography and (b) phase image] and methyl formate [(c) topography and (d) phase image].

ATR−FTIR Measurements. All experiments were performed on a Nicolet Nexus 870 spectrometer equipped with an attenuated total reflectance cell (ATR Smart ARK accessory) with a ZnSe window, a XT-KBr beam splitter, and a DTGS-TEC detector. The samples were placed directly on the ZnSe window, and the spectra were acquired with a resolution of 4 cm^{-1} and an average of 128 scans, from which a background was subtracted. All spectra were Fourier transformed, processed with a Happ-Genzel apodization function,

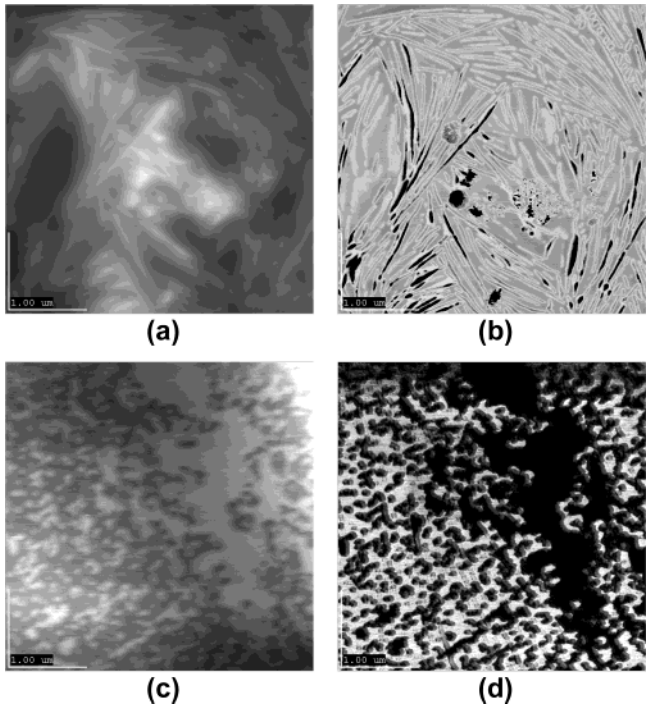

Figure 3. 4 μm × 4 μm AFM images of a PEO:$LiClO_4$ 20:1 film grown from acetonitrile [(a) topography and (b) phase image] and methyl formate [(c) topography and (d) phase image].

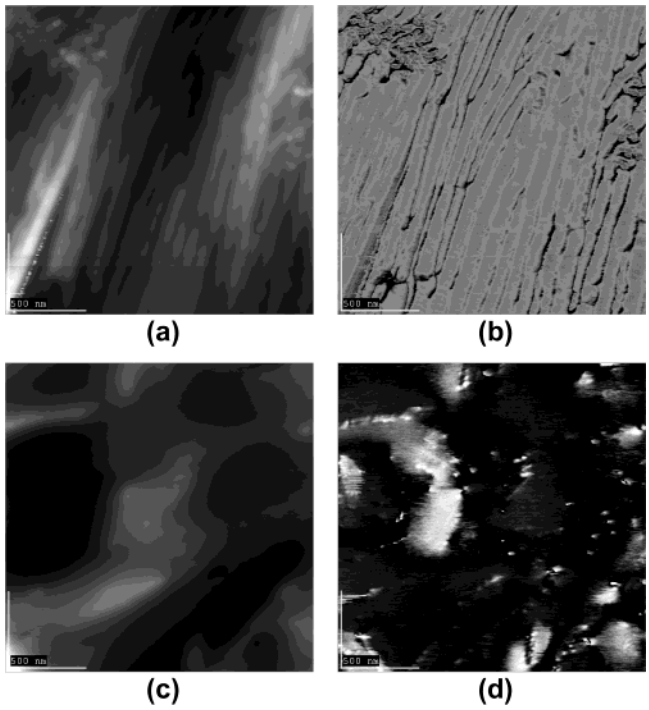

Figure 4. 2 μm × 2 μm AFM images of a PEO:$LiBF_4$ 20:1 film grown from acetonitrile [(a) topography and (b) phase image] and methyl formate [(c) topography and (d) phase image].

a Mertz phase correction, and normalized by dividing to their maximum intensity.

Conductivity Measurements. Two film-covered circular stainless plates were sandwiched into a button cell-type assembly, sealed, and placed into a variable temperature control bath (VWR Scientific). An impedance meter (HP series) operating at a frequency between 0.001 Hz and 13 kHz was used over the temperature range between 25 and 80 °C in the

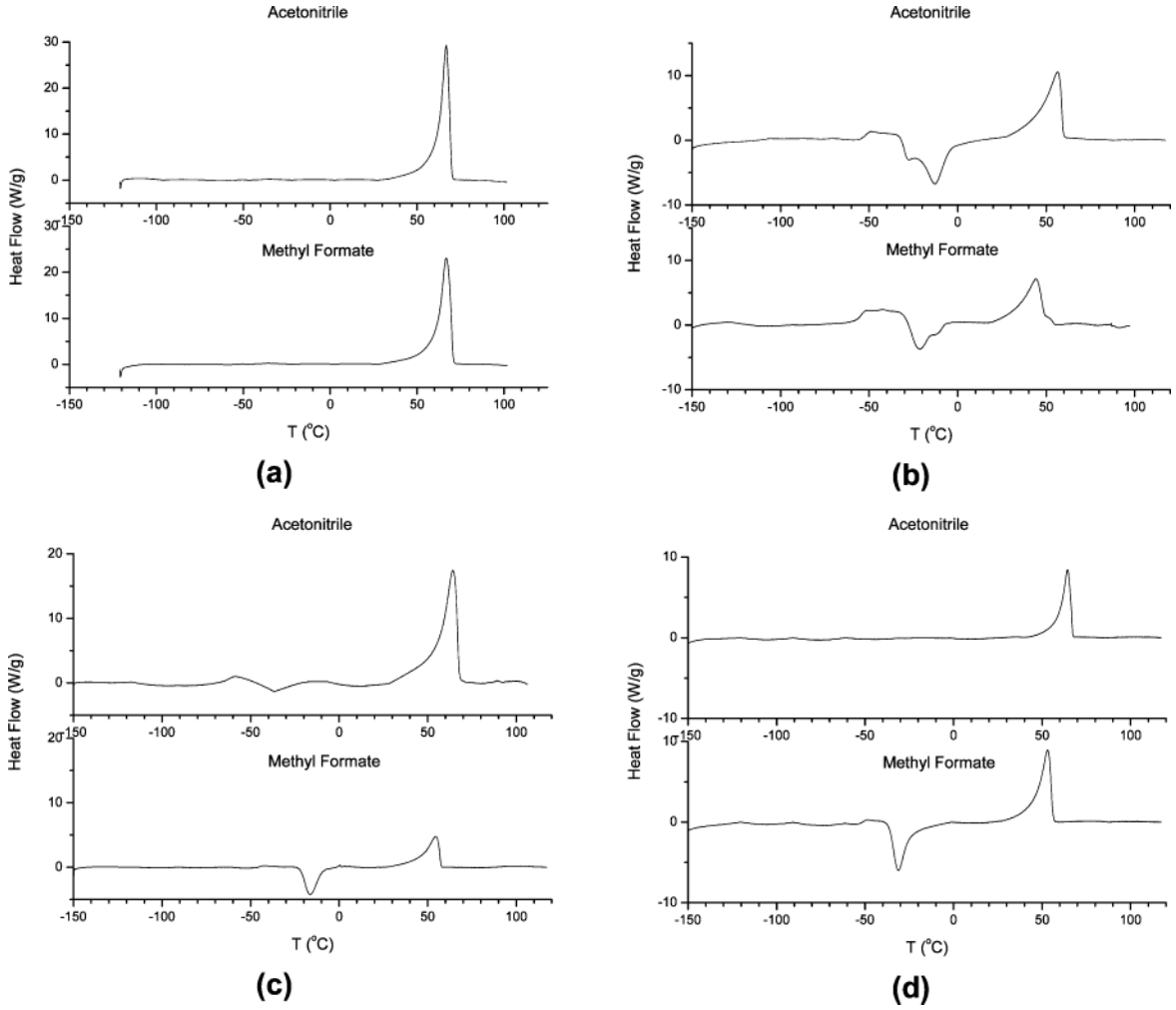

Figure 5. DSC heating scans (after quenching) of (a) pristine PEO and 20:1 (b) PEO:LiTFSI, (c) PEO:$LiClO_4$, and (d) PEO:$LiBF_4$, films grown from both solvents.

cooling and heating regimes, allowing an equilibrium time of 20 min at each measurement temperature. The conductivity values were extracted from the following equation:

$$K = \frac{1}{R}\frac{L}{A} \tag{1}$$

where K is the conductivity, R the measured resistance on the impedance curve, A the area of the circular stainless plates ($A = \pi r^2$), and L the distance between them. L can be evaluated as the film thickness calculated from subtracting the thickness of the free plates to the one of the assembly after cycling. Thicknesses were measured with a Mitutoyo electronic micrometer.

PFGSE−NMR Measurements. A homemade spectrometer equipped with a superconducting coil providing a direct magnetic field of 6.6 T was used. For diffusion measurements we applied a pulsed magnetic field gradient technique (PMFG) with spin echo (SE) using the pulse sequence ($\pi/2$, τ, π) described by Stejskal and Tanner.[20] The diffusion coefficient of a species can be determined as $A^*(2\tau)$, the amplitude of the echo signal at the time 2τ, is proportional to the square of the applied gradient (g^2) following the equation:

$$\ln\left[\frac{A^*(2\tau)}{A(2\tau)}\right] = -\gamma^2 D\delta^2\left(\Delta - \frac{\delta}{3}\right)g^2 \tag{2}$$

where $A(2\tau)$ is the amplitude of the echo signal with no applied gradient, γ the gyromagnetic ratio for a given nucleus, D the diffusion coefficient of the probed species, δ the time duration of the pulse gradient, and Δ the time interval between two gradient pulses. The maximum gradient pulses delivered by a Techtron power supply was 56 A for 5 ms, giving a $g_{max} =$ 1000 G/cm. The free induction decay (FID) curve, due to transverse (or spin−spin) relaxation with a characteristic time (T_2), was reconstructed by measuring the amplitude of the echo signal for different τ values. The measured echo amplitude, for each τ value, was normalized to the maximum intensity at $\tau = 0$. More details on these types of measurements can be found elsewhere.[21]

The "NMR conductivity", σ_{NMR}, was obtained using the Nernst−Einstein equation:

$$\sigma_{NMR} = Ne^2\frac{D^+ + D^-}{kT} \tag{3}$$

where D is the diffusion coefficient of the species (the superscripts (+) and (−) refer to the cation and anion, respectively), e the elementary charge, k the Boltzmann constant, T the temperature, and N the number of carriers per cm^3. N was evaluated for the PEO:LiTFSI 20:1 complex by using the equation

$$N = \frac{\rho N_A}{20M_{EO} + M_{LiTFSI}} \tag{4}$$

where the density of PEO is known to be $\rho = 1.3$ g/cm^3, N_A is the Avogadro constant, M_{EO} is the molar mass of the EO unit in PEO, and M_{LiTFSI} is the molar mass of LiTFSI.

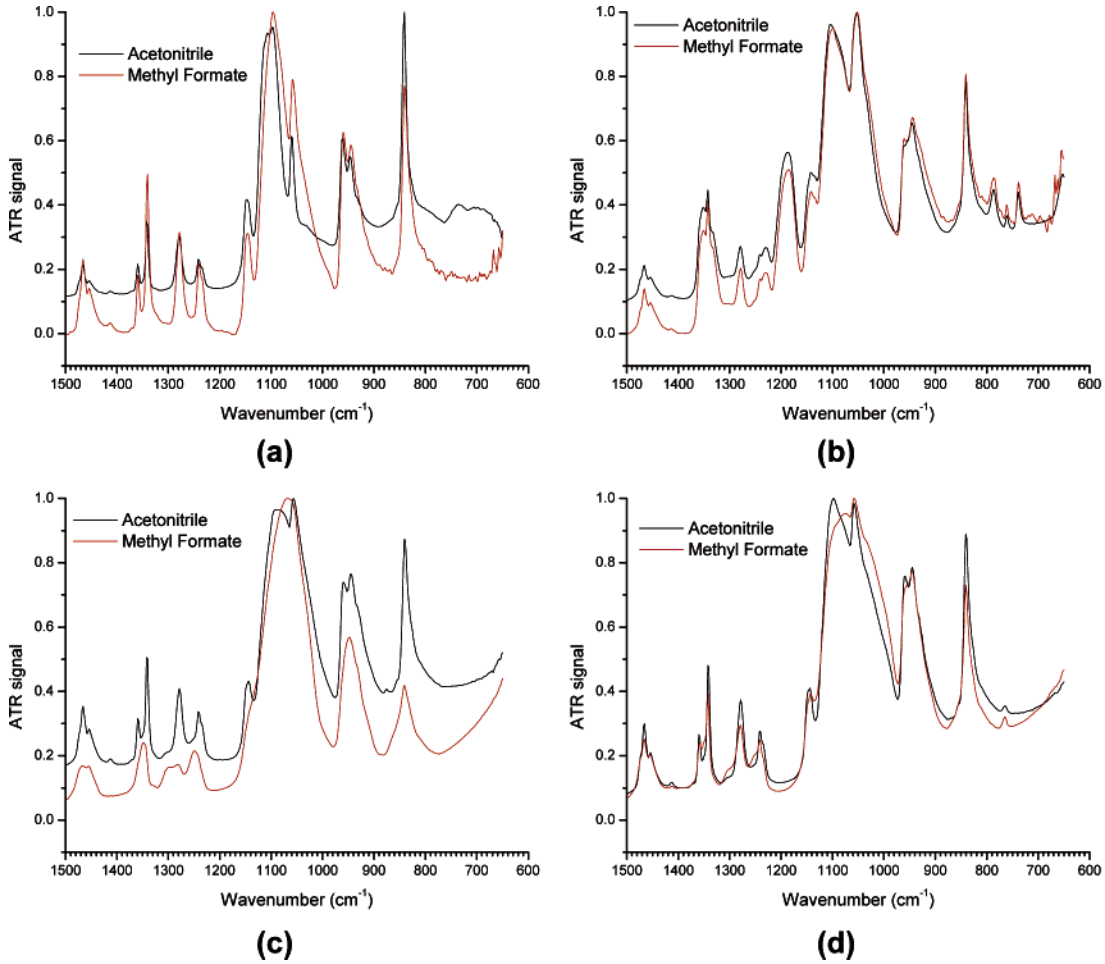

Figure 6. ATR−FTIR spectra of (a) pristine PEO and 20:1 (b) PEO:LiTFSI, (c) PEO:$LiClO_4$, and (d) PEO:$LiBF_4$, films grown from both solvents.

The transport numbers, t, were extracted from the diffusion coefficients, D, following the equations

$$t^+ = \frac{D^+}{D^+ + D^-} \tag{5}$$

$$t^+ + t^- = 1 \tag{6}$$

Results and Discussion

We first examined the pristine poly(ethylene oxide) films. From Figure 1, we can see that the AFM images of the plain polymer are clearly different depending on the solvent used to prepare the films. PEO films grown from AN show fiberlike features whereas from MF, they display agglomerates. Acetonitrile is known to be a good solvent with a Hildebrand solubility parameter $\delta = 24.4$ $J^{1/2}$ $cm^{3/2}$ (as an indication $\delta = 14.9$ $J^{1/2}$ $cm^{3/2}$ for hexane and $\delta = 47.9$ $J^{1/2}$ $cm^{3/2}$ for water) and a dielectric constant $\epsilon = 37.5$. While less known, MF is a poor solvent of PEO due to its low dielectric constant ($\epsilon = 8.5$). Both closer homologues, methyl acetate ($\epsilon = 6.7$) or ethyl formate ($\epsilon = 7.1$), are nonsolvents of PEO.

In AN, the polymer chains will tend to expand to favor interactions with the solvent. In MF, it is the opposite case; PEO will tend to coil in order to minimize chain interactions with the solvent. In all cases, on the basis of the Flory theory of solvation,[22] in θ solvents, the polymer chains will reach dimensions (within the limits of their restricted rotations) where the expanding tendency of the chain is compensated by the agglomerative effect of attractive polymer chain neighbors. In the case of a poor solvent, it is obvious that the expanding tendency of the chain will be minimized and the polymer chain attractions maximized. Our experimental observations were that the PEO solutions in MF took more time to become homogeneous than for AN, despite the higher viscosity of the latter. In some cases, it was even necessary to slightly heat the MF solutions until the θ temperature is reached in order for the polymer to dissolve, which can be seen as the time when the chains occupying a minimum volume start to entangle.

Even after salt is added, this cooperative agglutination is evident for the MF grown films in the presence of LiTFSI (Figure 2), $LiClO_4$ (Figure 3), and $LiBF_4$ (Figure 4). The opposite case is observed for the AN grown films where the breathing fibrous features remain.

The DSC data (Figure 5) show no relevant differences between the two solvents for the pristine PEO samples (Figure 5a). Nevertheless, when salt is added, it is possible to see some differences. Transition temperatures (glass transition, crystallization, and fusion) occur a couple of degrees higher for the AN grown samples compared to their MF counterparts (Figure 5b−d). Even more interesting, for the PEO:$LiClO_4$ (Figure 5c) and PEO:$LiBF_4$ (Figure 5d) samples it is possible to see a crystallization event for the MF samples (around −17 °C for PEO:$LiClO_4$ and −32 °C for PEO:$LiBF_4$), whereas

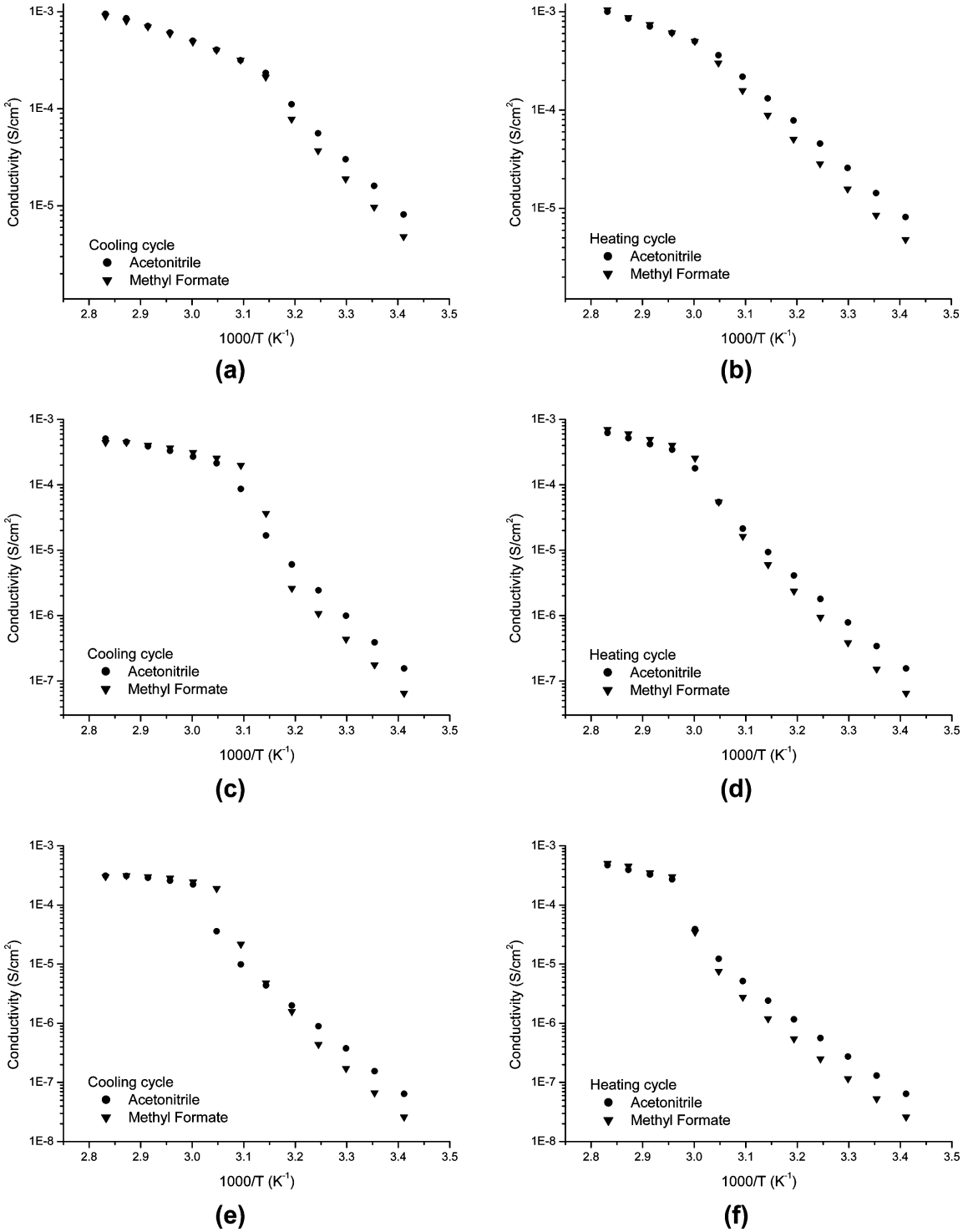

Figure 7. Conductivity during cooling and heating cycles for 20:1 complexes of: PEO:LiTFSI [(a) and (b)], PEO:$LiClO_4$ [(c) and (d)], and PEO:$LiBF_4$ [(e) and (f)], cast from the two solvents.

no noticeable crystallization seems to be occurring for the AN samples. To be sure that there were no major salt concentration differences and no chemical events due to the solvent or even some remaining trapped solvent even after drying, we recorded ATR−FTIR spectra of all the dry samples. From Figure 6, we observe neat spectra with highly superimposable bands which are similar to those extensively examined by Servant and co-workers.[23,24]

On the basis of these observations, it is obvious that the polymer has a spatial memory of the solvent (as seen by AFM), which in turn affects the chain dynamics implied in the transition events seen in the DSC data in the presence of either lithium salt. To investigate further this structure/property relationship, we measured the conductivity of all the PEO−lithium salt complexes (Figure 7). The knee where there is a change of slope in all the curves corresponds to the melting point of each complex. In both heating and cooling scans, when the PEO−lithium salt complexes are totally melted, there is no pronounced difference whether the films were grown out of either solvent. At this stage, the preservation of nonconductive domains of stoichiometric 6:1 complexes can be ruled out considering the

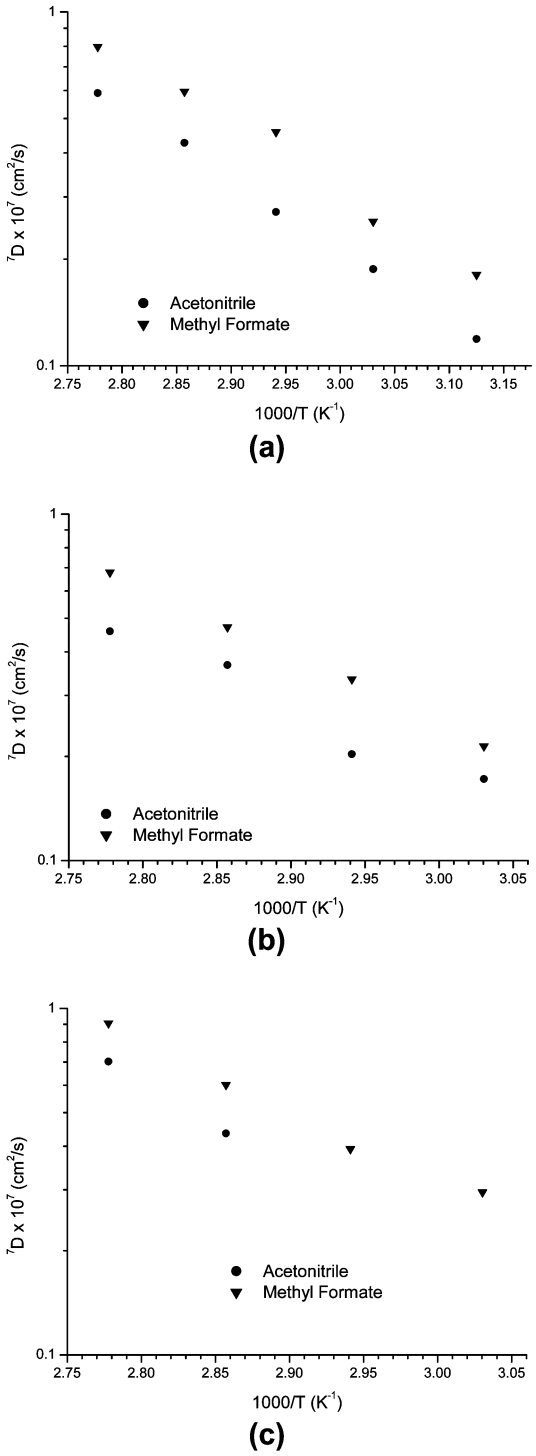

Figure 8. ^{7}Li diffusion coefficients (^7D), as measured by PFGSE−NMR, for films of: 20:1 (a) PEO:LiTFSI, (b) PEO:$LiClO_4$, and (c) PEO:$LiBF_4$, grown from both solvents.

low melting temperatures of both type of samples at this composition. It starts to get interesting at temperatures lower than the melting transition. Films that were in the presence of MF are less conductive than the ones that met AN by a factor comprised between 1.1 and 1.7 for PEO:LiTFSI, 1.3 and 2.4 for PEO:$LiClO_4$, and 1.1 and 2.5 for PEO:$LiBF_4$. This noticeable effect is independent of the scan direction (heating or cooling).

By looking at the ^{7}Li diffusion coefficients measured by PFGSE−NMR for all the samples (Figure 8), one can see that lithium diffuses appreciably and systematically faster in the MF-grown films compared to the AN ones.

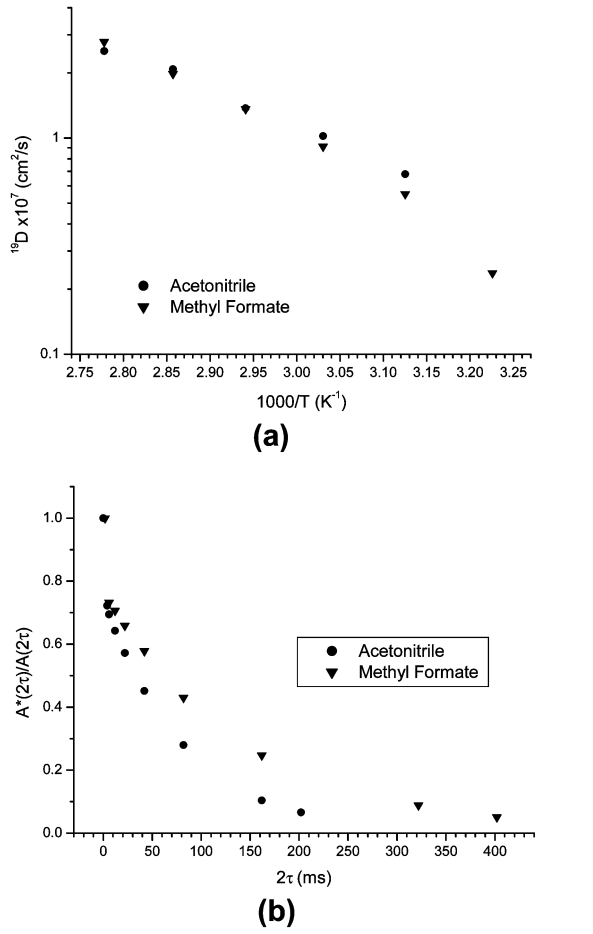

Figure 9. ^{19}F (a) diffusion coefficient and (b) free induction decay, with a time constant (T_2), as measured by PFGSE-NMR, for films of 20:1 PEO:LiTFSI grown from both solvents.

Because of their solvent-affected spatial organization, PEO chains in the MF films must have a wider free volume distribution than the AN ones and hence favor a faster lithium ion diffusion. For the case of PEO:LiTFSI, the ^{19}F diffusion coefficient and the free induction decay curves are shown in Figure 9. Conversely, there is little influence of the sample history on D^-, with even slightly higher values for the AN-processed sample (Figure 9a). Noteworthy, even if the difference is small, the variations with temperature are different with a crossover of the curves at ≈66 °C. Moreover, Figure 9b shows a faster decay for the AN curve, indicative of faster dynamics in this sample. We did not succeed in measuring the diffusion coefficient of either F or B in the BF_4^- anion as no detectable echo signal could be achieved in the current samples. In the case of the ClO_4^- anion, there is no nucleus that could be probed.

To discuss the apparent paradox of a higher diffusivity, at least for the cations, and lower conductivity for the MF vs AN samples, we show in Table 1 the calculated conductivity (σ_{NMR}) from the Nernst−Enstein equation (3) and the ratio $\alpha = \sigma_{measured}/\sigma_{NMR}$. Since NMR is not charge sensitive, it probes the motion of species that do not contribute to the conductivity (like ion pairs), and α is a measure of the dissociation. At all temperatures, except one, $\alpha_{AN} \approx 1 > \alpha_{MF}$. The only temperatures where $\alpha_{AN} \approx \alpha_{MF} < 1$ are around 60 °C, the melting point, and the effect is thus unconclusive. The almost total dissociation of LiTFSI in polymer electrolytes is

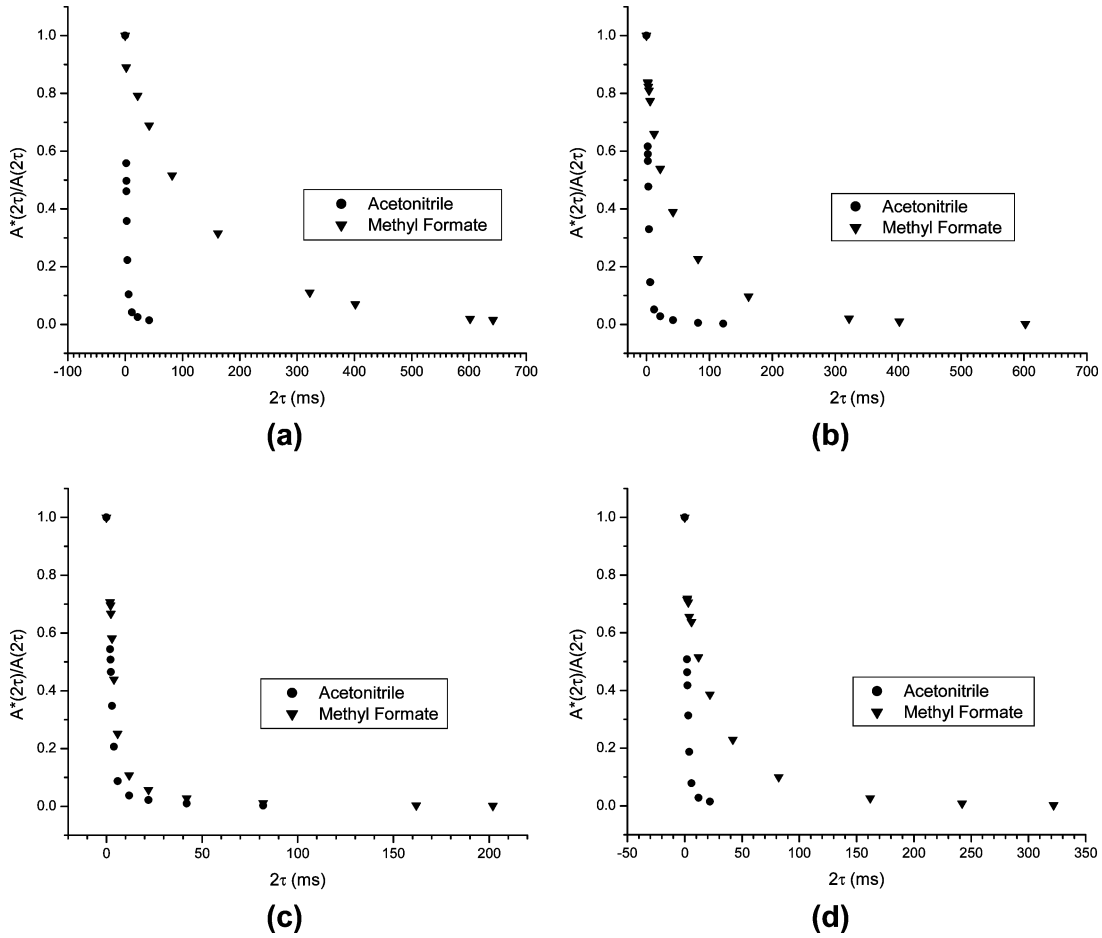

Figure 10. ^{1}H free induction decay, with a time constant (T_2), as measured by PFGSE-NMR, for films of (a) pristine PEO and 20:1 (b) PEO:LiTFSI, (c) PEO:$LiClO_4$, and (d) PEO:$LiBF_4$, grown from both solvents.

Table 1. Conductivity (Measured and Extracted from NMR Data during Cooling Cycles) and Transport Numbers for the PEO:LiTFSI 20:1 Complex Cast from Acetonitrile (AN) and Methyl Formate (MF)

	T = 360 K		T = 350 K		T = 340 K		T = 330 K		T = 320 K	
	AN	MF	AN	MF	AN	MF	AN	MF	AN	MF
$\sigma_{measured}$, S cm^{-1} × 10^4	9.46	9.03	8.52	8.02	6.08	5.93	4.06	4.01	2.33	2.12
σ_{NMR}, S cm^{-1} × 10^4	10.8	12.4	8.92	9.17	6.02	6.67	4.56	4.41	3.11	2.85
$\sigma_{measured}/\sigma_{NMR}$	0.876	0.728	0.955	0.875	1.01	0.889	0.890	0.909	0.749	0.744
t^+	0.190	0.223	0.170	0.231	0.166	0.252	0.155	0.219	0.149	0.248
t^-	0.810	0.777	0.830	0.769	0.834	0.748	0.845	0.781	0.851	0.752

expected from the "hyper-delocalization" of this anion and has been verified by different spectroscopic[6,23,25] and neutron techniques.[26,27] (Interestingly, the corresponding samples have invariably been made from AN solutions.) The salt seems to be much less dissociated when coming from a MF-based preparation as apparent in Table 1. Thus, a lower number of carriers contribute to the lower conductivity of these electrolytes. The same phenomenon must be occurring for $LiClO_4$ and $LiBF_4$ (Figure 7c−f) and PFGSE−NMR measurements on $^{10}BF_4^-$ are underway to further assess the BF_4^- anion. The higher dielectric constant of AN compared to MF (as mentioned above), meaning higher dissociation, seems to be memorized in the polymer resulting from evaporation of these solvents.

A set of very important parameters in polymer electrolytes are the transport numbers t^+ and t^-: the respective fraction of current carried by cations and anions. A high t^+ is desirable as it controls the deleterious concentration gradient which appears when using Li-exchanging electrodes (Li°, intercalation materials), as in batteries. A slight variation in t^+ has a profound influence on the current-carrying capability.[28] Table 1 is explicit; for the PEO:LiTFSI system, t^+_{MF} is appreciably higher than t^+_{AN} and is also almost independent of temperature while t^+_{AN} decreases steadily with the lowering of temperature. Following eq 6, these lower t^+_{AN} values are compensated by higher t^-_{AN} values (Table 1).

These differences are further confirmed by the ^{1}H free induction decay curves (Figure 10). We can see from the data that the FID curves reach zero faster for the AN vs MF grown samples, in all cases (pristine PEO or PEO complexes with a lithium salt). This rapid decay, observed for the samples that were in contact with AN, suggests that the PEO rotational and/or translational relaxation dynamics[27] are faster for these samples. PEO must in these cases adopt conformations that favor fast segmental motions which expectedly translates into higher conductivities, however mostly allowed to the anion as revealed by the higher t^-_{AN} values (Table 1). Future neutron scattering work on films grown from both solvents will allow us to probe, with high accuracy, the time scales of these relaxation dynamics.

Conclusions

The results reported here show without ambiguity that all the relevant properties of polymer electrolytes are affected by the sample history: in this particular case the solvent from which the complex was prepared. Morphology is strikingly different, while conductivity is affected more modestly: the variation being comparable to that observed when for instance nanoparticle fillers are added to the polymer electrolyte or when it is put under mechanical strain. More important is the variation in transport numbers with its consequences on the performances of polymer electrolytes under current-carrying conditions. This is the first report of a possible manipulation and control of this parameter. It opens new possibilities with different solvents or solvent mixtures.

It is quite remarkable that the "memory effect" is stable not only with time but also with repeated temperature excursions beyond the full amorphization (melting point) of the samples. It would have been expected that reptation would eventually bring the two sets of samples to similar equilibrium. This suggests that the ions act, as a whole, as cross-links for the polymer.

In all cases, the effect is important enough to suggest that future work on polymer electrolytes gives precisely the preparation conditions and that previous work should be scrutinized for variations in sample history.

Acknowledgment. The authors are grateful to the French government, through Madame Dominique Sotteau from the General Consulate of France in Montréal, for providing an EGIDE scholarship to M.V. for the NMR experiments at the Université Joseph Fourier.

References and Notes

(1) Berthier, C.; Gorecki, W.; Minier, M.; Armand, M.; Chabagno, J.-M.; Rigaud, P. *Solid State Ionics* **1983**, *11*, 91.
(2) Watanabe, M.; Nagano, S.; Sanui, K.; Ogata, N. *Solid State Ionics* **1986**, *18/19*, 338.
(3) Lascaud, S.; Perrier, M.; Vallée, A.; Besner, S.; Prud'homme, J. *Macromolecules* **1994**, *27*, 7469.
(4) Tarascon, J. M.; Armand, M. *Nature (London)* **2001**, *414*, 359.
(5) Gray, F. M.; MacCallum, J. R.; Vincent, C. A. *Solid State Ionics* **1986**, *18/19*, 282.
(6) Gorecki, W.; Roux, C.; Clémancey, M.; Armand, M.; Belorizky, E. *ChemPhysChem* **2002**, *7*, 620.
(7) Weston, J. E.; Steele, B. C. H. *Solid State Ionics* **1982**, *7*, 75.
(8) Croce, F.; Appetecchi, G. B.; Persi, L.; Scrosati, B. *Nature (London)* **1998**, *394*, 456.
(9) Strümpler, R.; Glatz-Reichenbach, J. *J. Electroceram.* **1999**, *3*, 329.
(10) Zhou, J.; Fedkiw, P. S. *Solid State Ionics* **2004**, *166*, 275.
(11) Gadjourova, Z.; Andreev, Y. G.; Tunstall, D. P.; Bruce, P. G. *Nature (London)* **2001**, *412*, 520.
(12) Zheng, Y.; Chia, F.; Ungar, G.; Wright, P. V. *Chem. Commun.* **2000**, 1459.
(13) Chia, F.; Zheng, Y.; Liu, N.; Reeves, N.; Ungar, G.; Wright, P. V. *Electrochim. Acta* **2003**, *48*, 1939.
(14) Itoh, T.; Hirata, N.; Wen, Z.; Kubo, M.; Yamamoto, O. *J. Power Sources* **2001**, *97*−*98*, 637.
(15) Golodnitsky, D.; Peled, E. *Electrochim. Acta* **2000**, *45*, 1431.
(16) Golodnitsky, D.; Livshits, E.; Rosenberg, Y.; Lapides, I.; Peled, E. *Solid State Ionics* **2002**, *147*, 265.
(17) Vorrey, S.; Teeters, D. *Electrochim. Acta* **2003**, *48*, 2137.
(18) Hubbard, H. V.; Sills, S. A.; Davies, G. R.; McIntyre, J. E.; Ward, I. M. *Electrochim. Acta* **1998**, *43*, 1239.
(19) Cable, K. M.; Mauritz, K. A.; Moore, R. B. *Chem. Mater.* **1995**, *7*, 1601.
(20) Stejskal, E. O.; Tanner, J. E. *J. Phys. Chem.* **1965**, *42*, 288.
(21) Gorecki, W.; Jeannin, M.; Belorizky, E.; Roux, C.; Armand, M. *J. Phys.: Condens. Matter* **1995**, *7*, 6823.
(22) Flory, P. J. *Principles of Polymer Chemistry*; Cornell University Press: Ithaca, NY, 1953.
(23) Rey, I.; Lassègues, J. C.; Grondin, J.; Servant, L. *Electrochim. Acta* **1998**, *43*, 1505.
(24) Ducasse, L.; Dussauze, M.; Grondin, J.; Lassègues, J. C.; Naudin, C.; Servant, L. *Phys. Chem. Chem. Phys.* **2003**, *5*, 567.
(25) Bakker, A.; Gejji, S.; Lindgren, J.; Hermansson, K.; Probst, M. M. *Polymer* **1995**, *36*, 4371.
(26) Mao, G.; Saboungi, M.-L.; Price, D. L.; Armand, M. B.; Howells, W. S. *Phys. Rev. Lett.* **2000**, *84*, 5536.
(27) Mao, G.; Saboungi, M.-L.; Price, D. L.; Armand, M.; Mezei, F.; Pouget, S. *Macromolecules* **2002**, *35*, 415.
(28) Doyle, M.; Fuller, T. F.; Newman, J. *J. Electrochem. Soc.* **1993**, *140*, 1526.

MA0490404